

# Efficient qubit detection using alkali earth ions and a double STIRAP process

Ditte Møller,\* Jens L. Sørensen, Jakob B. Thomsen, and Michael Drewsen  
*QUANTOP - Danish National Research Foundation Center for Quantum Optics,  
 Department of Physics and Astronomy, University of Aarhus, DK-8000, Denmark.*

(Dated: March 13, 2022)

We present a scheme for robust and efficient projection measurement of a qubit consisting of the two magnetic sub-levels in the electronic ground state of alkali earth ions. The scheme is based on a double STIRAP process involving four partially coherent laser fields. We show how the efficiency depends on experimentally relevant parameters: Rabi frequencies, pulse widths, laser line widths, one- and two photon detunings, residual laser power, laser polarization and ion motion.

PACS numbers: 03.67.Lx, 32.80.Qk, 39.30.+w

## I. INTRODUCTION

Quantum computation holds the promise of potentially efficient solving of many problems being of high complexity for known classical algorithms [1]. Currently, efforts are made within many fields of physics in order to explore the possibility of realizing quantum computing. Notable examples are superconducting circuits [2, 3], semiconductors [4], linear optics with single photons [5, 6], cold neutral atoms in cavities [7] and lattices [8, 9, 10] as well as cold, trapped ions [11]. So far, most progress has been made in ion trap systems, where quantum gates [12, 13], many qubit entanglement [14, 15] and quantum error correction has been demonstrated [16].

The most successfully qubit states implemented with trapped ions are two hyperfine components of the  ${}^9\text{Be}^+$  ground state [12] and a combination of the metastable  $3\text{D}_{5/2}$  state and the  $4\text{S}_{1/2}$  states in  ${}^{40}\text{Ca}^+$  [13]. In both cases linear Paul traps are used to confine the ions. As a qubit we consider in this work the electron spin in the alkali earth ion ground state. In Fig. 1 the electronic ground state is denoted  $|1\rangle$  and the qubit basis is denoted  $|\uparrow\rangle$  and  $|\downarrow\rangle$ . Single qubit operations as well as gate operations can e. g. be performed by driving stimulated Raman transitions between the two qubit states [17], or, alternatively using controlled mechanical light forces [18]. Since only ground states are involved, the qubit decoherence will be limited only by ambient noise fields and ion heating effects, rather than the excited state lifetimes. One does, however, face the problem of detecting the qubit state in an efficient manner. Toward this end we present in this paper a scheme for potentially efficient qubit projective measurements via shelving of population of one qubit state in the long lived metastable  $\text{D}_{5/2}$  state found in all alkali earth ions heavier than  $\text{Mg}^+$ .

As illustrated in Fig. 1, the qubit shelving is performed via a double Stimulated Raman Adiabatic Passage (STIRAP) process [19, 20]. Initial and final states of the shelving process are denoted  $|\downarrow\rangle$  and  $|5\rangle$  respectively. After shelving, the atomic population remaining in the  $|\uparrow\rangle$

state can be observed directly by resonantly driving the  $|1\rangle \rightarrow |2\rangle$  and  $|3\rangle \rightarrow |2\rangle$  transitions and monitoring the fluorescence [21]. We use the first STIRAP process to transfer the population from  $|\downarrow\rangle$  to  $|3\rangle$ , where we achieve the spin-state selectivity by using circularly right handed polarized light. The second process transfers the population from  $|3\rangle$  to the non-fluorescent  $|5\rangle$ -state. A weak externally applied magnetic field defines the quantization axis.

STIRAP has been shown to be a robust way of adiabatically transferring population from one quantum state to another in a three level lambda-system using two laser pulses in a counterintuitive order [20, 22, 23, 24, 25, 26, 27, 28, 29]. Compared to population transfer via  $\pi$ -pulses or rapid adiabatic passage, STIRAP has the advantage that no strict control of laser amplitude and phase is re-

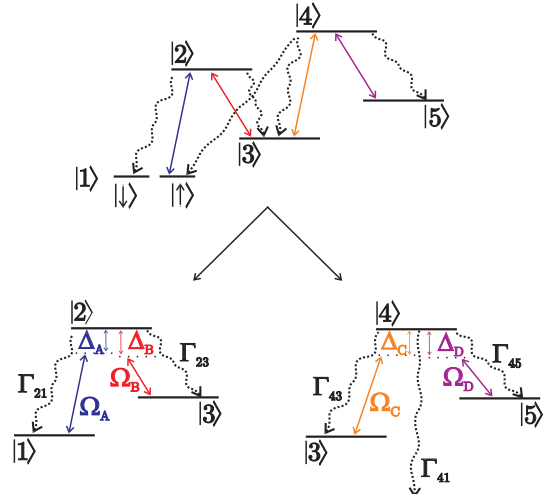


FIG. 1: (Color) Relevant energy levels of the alkali earth ions heavier than  $\text{Mg}^+$ . We consider the qubit encoded in the Zeeman sublevels,  $|\uparrow\rangle$  and  $|\downarrow\rangle$  of the electronic ground state,  $|1\rangle$ . The states  $|3\rangle$  and  $|5\rangle$  are metastable with lifetimes varying from a fraction of a second to many seconds depending on the ion species. The decay of these states is neglected here. Since the presented scheme consists of two stages of STIRAP, we break down the 5 level system into two 3 level  $\Lambda$  systems, each coupled by two optical fields.

\*Electronic address: dittem@phys.au.dk

quired to maintain a high efficiency [30]. However, STIRAP does require the pairs of laser pulses involved to be phase coherent relative to each other. In practice this means that either the lasers must be mutually phase locked or that the laser pulses must be sufficiently short, so that laser decoherence can be neglected. Of course decoherence is always at play, hence, in the calculations below we assume finite laser line widths and only partially coherent lasers.

The goal of this work is to theoretically investigate the shelving process and identify the parameters of importance to its efficiency. In Sec. II we first make some general remarks on the STIRAP-process. This treatment is valid for any three level  $\Lambda$  system and it serves to develop the criteria for maintaining adiabaticity using Gaussian shaped pulses. We then consider the roles of one- and two photon detunings of the Raman resonances, laser line widths, laser pulse widths, Rabi frequencies, stray laser light, laser polarizations and ion motion in Sec.'s IV and V. Here we use as an example the  $^{40}\text{Ca}^+$  ion, but, apart from different decay rates and wavelengths, our treatment is in general valid for any alkali earth ion or other ion system with energy levels consistent with Fig. 1. Finally we conclude in Sec. VII.

## II. STIRAP WITH GAUSSIAN PULSES

Let us first consider one STIRAP process involving three atomic basis states  $\{|1\rangle, |2\rangle, |3\rangle\}$ . In this section we will neglect spontaneous decay of the  $|2\rangle$  state, since this is of no importance to adiabaticity. Two mutually coherent and monochromatic laser fields  $A$  (pump field) and  $B$  (Stokes field) couples  $|1\rangle$  and  $|3\rangle$  to  $|2\rangle$  respectively (See Fig. 2). The interaction Hamiltonian for this system in the rotating wave approximation is given by

$$H_I(t) = \frac{\hbar}{2} \begin{pmatrix} 0 & \Omega_A(t) & 0 \\ \Omega_A(t) & 2\Delta_A & \Omega_B(t) \\ 0 & \Omega_B(t) & 2(\Delta_A - \Delta_B) \end{pmatrix} \quad (1)$$

where  $\Delta_A$  and  $\Delta_B$  are the detunings of the two applied fields having the real, time dependent Rabi frequencies,  $\Omega_A(t)$  and  $\Omega_B(t)$  respectively. These parameters are defined equivalent to ref. [20]. On two-photon resonance,

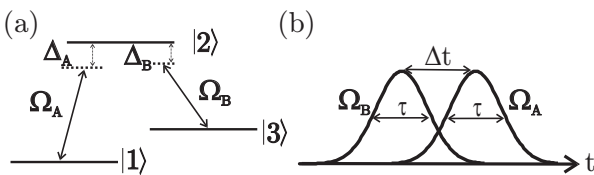


FIG. 2: Three-level lambda-system with a pump laser (A) and a Stokes laser (B) applied. The two laser fields have Rabi frequencies,  $\Omega_A$  and  $\Omega_B$  and they are detuned  $\Delta_A$  and  $\Delta_B$  from resonance.

$\Delta_A - \Delta_B = 0$ , diagonalizing (1) yields the eigenvalues

$$\omega^\pm = \frac{1}{2}(\Delta_A \pm \sqrt{\Delta_A^2 + \Omega_A^2 + \Omega_B^2}) , \quad \omega^d = 0, \quad (2)$$

corresponding to eigenstates

$$\begin{aligned} |+\rangle &= \sin(\alpha) \sin(\beta) |1\rangle + \cos(\beta) |2\rangle - \cos(\alpha) \sin(\beta) |3\rangle, \\ |-\rangle &= \sin(\alpha) \cos(\beta) |1\rangle - \sin(\beta) |2\rangle + \cos(\alpha) \cos(\beta) |3\rangle, \\ |d\rangle &= \cos(\alpha) |1\rangle - \sin(\alpha) |3\rangle, \end{aligned} \quad (3)$$

with  $\tan(\alpha) = \frac{\Omega_A(t)}{\Omega_B(t)}$  and  $\tan(\beta) = \sqrt{-\frac{\omega^-}{\omega^+}}$ . The  $|d\rangle$ -state has zero interaction energy and is hence decoupled from light. As a result adiabatic following of this state will involve no population of the potentially short-lived  $|2\rangle$ -state. Now, with all population initially in  $|1\rangle$  and only the Stokes field applied, this initial state is  $|d\rangle$ . Adiabatically decreasing  $\Omega_B$  while increasing  $\Omega_A$  corresponds to a variation of  $\tan(\alpha)$  from 0 to 1. This changes the dressed state,  $|d\rangle$ , from  $|1\rangle$  to  $|3\rangle$  after the pulse sequence.

Since STIRAP requires adiabatic following of atoms while remaining in the  $|d\rangle$ -state, we will now look at the criterion for this to happen. We assume essentially Fourier limited optical pulses with a Gaussian time dependence. These give rise to the time varying Rabi frequencies

$$\begin{aligned} \Omega_A(t) &= \Omega_{A,0} \exp \left[ -\left( \frac{t - \Delta t/2}{\tau/2} \right)^2 \right], \\ \Omega_B(t) &= \Omega_{B,0} \exp \left[ -\left( \frac{t + \Delta t/2}{\tau/2} \right)^2 \right] \end{aligned} \quad (4)$$

where the peak Rabi frequencies are  $\Omega_{A,0}$  and  $\Omega_{B,0}$ ,  $\Delta t$  is the pulse separation and  $\tau$  is the full width at  $1/e$  height, assumed to be the same for both pulses. We parameterize the problem in terms of the scaled time,  $\theta = \sqrt{8}t/\tau$ , scaled pulse separation,  $\eta = \sqrt{2}\Delta t/\tau$  and Rabi frequency asymmetry  $r = \Omega_{A,0}/\Omega_{B,0}$ . Hence

$$\begin{aligned} \Omega_A(\theta) &= \Omega_{A,0} \exp \left[ -1/2(\theta - \eta)^2 \right], \\ \Omega_B(\theta) &= \Omega_{B,0} \exp \left[ -1/2(\theta + \eta)^2 \right], \end{aligned} \quad (5)$$

and

$$|d\rangle = -\frac{r^{-1/2} e^{-\eta\theta} |1\rangle - r^{1/2} e^{\eta\theta} |3\rangle}{\sqrt{r e^{2\eta\theta} + r^{-1} e^{-2\eta\theta}}}. \quad (6)$$

Adiabaticity requires the rate of change of the wave function to be small compared to the energy separation between the dressed state eigenvalues,

$$\left| \frac{d}{dt} |d\rangle \right| \ll |\omega_\pm|. \quad (7)$$

The change of the wave function (6) we parameterize by the Bloch sphere polar angle in  $\{|1\rangle, |3\rangle\}$  basis, which

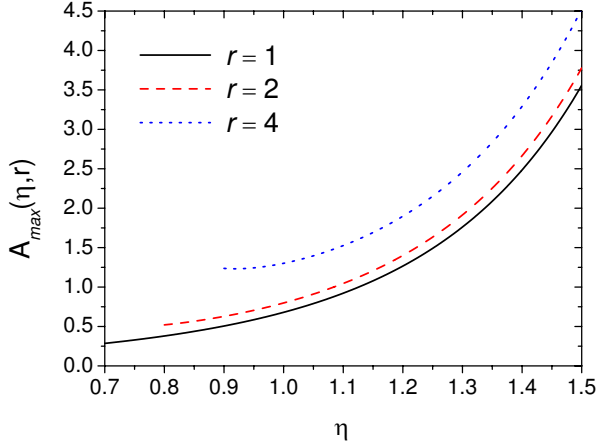


FIG. 3: (Color) Maximum value of the adiabaticity function,  $A_{max}(\eta, r) = A(\theta_{max}, \eta, r)$  as function of STIRAP pulse separation,  $\eta$ , for  $r = 1$ ,  $r = 2$  and  $r = 4$ . For  $r > 1$  a solution does not exist for smaller  $\eta$  values, hence the truncation of the corresponding curves. The maximum is found by solving Eq. (12).

from (3) and (6) is found to be  $\alpha = \arctan[r \exp(2\eta\theta)]$ . The wave function rate of change is then

$$\frac{d\alpha}{d\theta} = \frac{2\eta}{re^{2\eta\theta} + r^{-1}e^{-2\eta\theta}}. \quad (8)$$

This should be compared to the dimensionless eigenvalue of the energetically closest dressed state,  $|- \rangle$ . On two photon resonance and in the limit of large single photon detuning,  $\Omega_{A,0}, \Omega_{B,0} \ll |\Delta_A|$ , the eigenvalue is given by

$$\lambda_- = \frac{\omega^- \tau}{\sqrt{8}} = -2\Lambda (re^{2\eta\theta} + r^{-1}e^{-2\eta\theta}) \exp[-(\theta^2 + \eta^2)], \quad (9)$$

We can now formulate an adiabaticity criterion, which should be fulfilled at all times during the pulse sequence, where the Rabi frequencies are appreciable. The criterion states that

$$A(\theta, \eta, r) \equiv \frac{|\eta| \exp[\theta^2 + \eta^2]}{(re^{2\eta\theta} + r^{-1}e^{-2\eta\theta})^2} \ll \Lambda, \quad (10)$$

where we identify the parameter relevant for maintaining adiabaticity

$$\Lambda = \frac{\Omega_{A,0}\Omega_{B,0}}{16\sqrt{2}|\Delta_A|}\tau. \quad (11)$$

On inspection  $\Lambda$  is simply proportional to the product of the maximum achievable Raman Rabi frequency and the duration of the pulse sequence. Hence, Eq. (10) simply states that many Raman Rabi cycles should take place during the time span of the STIRAP process, analogous to the result derived in [20].

The timing of the STIRAP sequence is contained in the function  $A(\theta, \eta, r)$ . For a range of parameters

this has a maximum as function of time,  $A_{max}(\eta, r) = A(\theta_{max}, \eta, r)$ , where  $\theta_{max}$  solves the equation

$$2 \tanh(2\eta\theta_{max} + \ln r) = \theta_{max}/\eta. \quad (12)$$

For an efficient STIRAP process to occur, given a certain value of  $r$ , we obviously want to choose the pulse separation,  $\eta$ , so that  $A_{max}$  is small and obeying Eq. (10).

In Fig. 3 we plot  $A_{max}$  as function of  $\eta$  for values, where Eq. (12) has a solution. The three curves correspond to  $r = \{1, 2, 4\}$  and it should be noted that  $A_{max}(\eta, r) = A_{max}(\eta, r^{-1})$ . From the graphs we infer that values of  $\Lambda$  in excess of 3-5 should be obtained in order to ensure efficient population transfer. Adiabaticity is favored when the pulse separation is decreasing toward  $\eta = 0.7$  and when the Rabi frequencies are balanced, corresponding to  $r$  approaching unity. Given a certain time duration of the pulse sequence,  $\Theta$ , the population transfer efficiency in the adiabatic limit is found from Eq. (6) to be

$$P_3(\Theta) = [1 + r^{-2} \exp(-4\eta\Theta)]^{-1}. \quad (13)$$

As found experimentally [29] and shown in Sec. IV E, having a long time duration can pose a problem due to parasitic Raman resonances caused by residual light in actual experiments, hence the limitation set by a finite  $\Theta$  in (13) is indeed relevant. Obviously, (13) shows that the transfer efficiency grows with increasing  $\eta$ , due to the tails of the Gaussian pulses. However, since adiabaticity will suffer for larger  $\eta$ , we expect to find an optimum value of the pulse separation,  $\eta_{opt}$ , which depends only on  $r$  and  $\Lambda$ . With respect to  $r$  the efficiency grows for high values of  $r$ , while adiabaticity requires values close to  $r = 1$  and one therefore might expect an optimal value above 1 depending on  $\Lambda$ . To optimize the transfer efficiency with respect to  $\eta$  and  $r$ , we solve the optical Bloch equations for the three level  $\Lambda$  system. Details of our derivation of the Bloch equations can be found in the next section.

In order to make our Bloch equation solutions general we again ignore the decay from the short lived state  $|2\rangle$  and we assume perfectly coherent laser fields. The Bloch equations are integrated numerically for one photon detunings of 4 GHz. These detunings are chosen sufficiently large, so that for Rabi frequencies in the 100 MHz range, the results are independent of the specific values of the detunings. It is checked numerically that increasing the detunings even more has no impact on the solutions. In this limit our results can be considered general and system independent.

For fixed values of  $r$  and  $\Lambda$  the population transfer is computed as function of  $\eta$  and the optimum value,  $\eta_{opt}$ , corresponding to the maximum population transfer,  $P_{max}$ , is found. Examples of such curves can be found in Sec. IV A, where we analyze the sensitivity of the population transfer with respect to fluctuations of  $\eta$ . Fig. 4(a) shows  $\eta_{opt}$  as function of  $r$  for  $\Lambda = \{1, 3, 10\}$ . From the curves it is found that for values of  $r$  far from

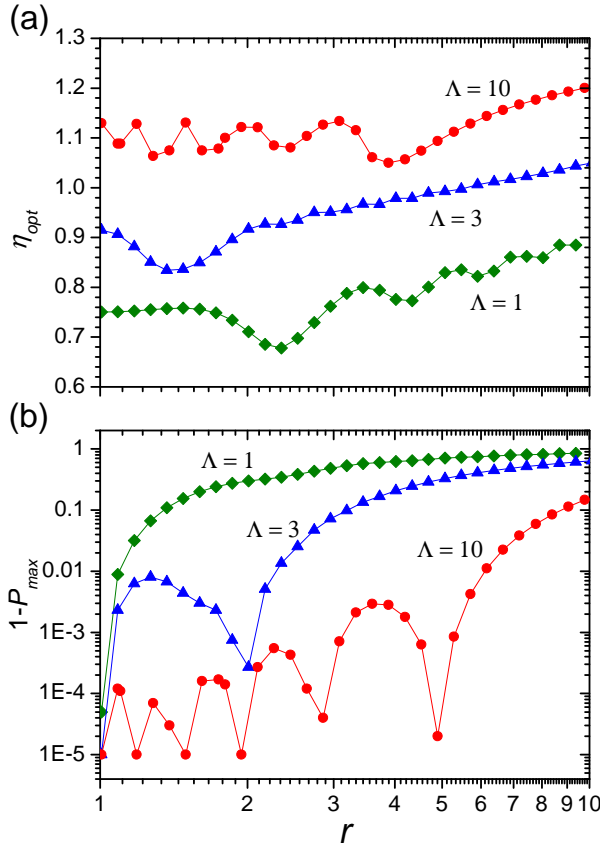


FIG. 4: (Color) (a) Optimum pulse separation,  $\eta_{opt}$  as function of Rabi frequency ratio,  $r = \Omega_{A,0}/\Omega_{B,0}$ . As indicated, the three curves correspond to different values of  $\Lambda$ , given by  $\Lambda = 1$  ( $\blacklozenge$ ),  $\Lambda = 3$  ( $\blacktriangle$ ) and  $\Lambda = 10$  ( $\bullet$ ). One-photon detunings are  $\Delta_A/2\pi = \Delta_B/2\pi = 4$  GHz and all results are obtained with  $\tau = 2$   $\mu$ s. (b) The transfer inefficiency  $1 - P_{max}$  corresponding to the values of  $\eta_{opt}$  calculated in (a). The oscillations of the curves are attributed to Rabi dynamics and it should be noted that the curves are symmetric with respect to letting  $r \rightarrow r^{-1}$ .

unity, a larger pulse separation is preferable. As mentioned above, this is attributed to the wings of the larger amplitude Gaussian pulse, which must decay ( $r < 1$ ) - or grow ( $r > 1$ ) sufficiently before the pulse sequence is terminated. This is also the reason why  $\eta_{opt}$  grows from about 0.7 for  $\Lambda = 1$  to about 1.1 for  $\Lambda = 10$ . Fig. 4(b) shows the population transfer inefficiency,  $1 - P_{max}$  associated with the values of  $\eta_{opt}$  computed in Fig. 4(a). From these curves it is obvious that balanced Rabi frequencies are crucial for an efficient population transfer when the adiabaticity criterion (10) is only marginally fulfilled, as it is the case for  $\Lambda = 1$ . As  $\Lambda$  grows, we see that higher asymmetries in the Rabi frequencies can be tolerated. This is in accordance with the discussion of Fig. 3. It should be noted that inclusion of finite laser line widths tends to make  $\eta_{opt}$  smaller as a result of decoherence mechanisms explained in Sec. IV C. For the remaining simulations in this paper we have tried to use

optimum values of  $\eta$  according to the reasoning above.

Although Fig. 4(b) shows that the fidelity of qubit detection in general is high for  $\Lambda = 10$ , it should be noted that the difference between a detection efficiency of  $10^{-3}$  and  $10^{-5}$  becomes very important when error correction protocols are considered [1]. Hence, optimizing fidelity with respect to  $r$ , according to Fig. 4(b), is crucial if the qubit detection scheme should be utilized for scalable quantum computation.

### III. OPTICAL BLOCH EQUATIONS

In order to investigate how robust the proposed detection scheme is against parameter fluctuations we now solve the optical Bloch equations describing the dynamics of the five levels depicted in Fig. 1 but ignore magnetic sublevels. We stay within the dipole approximation and define the Rabi frequencies

$$\Omega_A = \mu_{12} E_A / \hbar \quad (14)$$

$$\Omega_B = \mu_{32} E_B / \hbar \quad (15)$$

$$\Omega_C = \mu_{34} E_C / \hbar \quad (16)$$

$$\Omega_D = \mu_{54} E_D / \hbar \quad (17)$$

where  $\mu_{ij}$  are the dipole matrix elements and  $E_i$  laser field amplitudes. The laser fields with frequencies  $\omega_{ij}$  are not necessarily on resonance and we introduce detunings  $\Delta_{ij} = \frac{\mathcal{E}_i - \mathcal{E}_j}{\hbar} - \omega_{ij}$  with respect to the atomic energy levels  $\{\mathcal{E}_i\}$ . Linking up with the notation of Fig. 1 above we define  $\Delta_A = \Delta_{21}$ ,  $\Delta_B = \Delta_{23}$ ,  $\Delta_C = \Delta_{43}$  and  $\Delta_D = \Delta_{45}$ . Furthermore, we apply the rotating wave approximation to arrive at the interaction Hamiltonian for our system

$$H = \sum_{i=1}^5 \hbar \omega_i \rho_{ii} + (\hbar \Omega_A \rho_{12} + \hbar \Omega_B \rho_{32} + \hbar \Omega_C \rho_{34} + \hbar \Omega_D \rho_{54} + h.c.), \quad (18)$$

where  $\omega_i = \mathcal{E}_i / \hbar$  and the density operator elements are  $\rho_{ij} = |j\rangle \langle i|$ . Spontaneous emission is introduced as decay terms in the density matrix elements. We neglect spontaneous decay from the metastable  $|3\rangle$  and  $|5\rangle$  states because their lifetimes are significantly longer than the simulation time. Phase fluctuations of the lasers are introduced as decay of the coherences and ion micro-motion as a harmonic modulation of the detunings.

### IV. SIMULATIONS IGNORING ATOMIC SPIN

In the simulations we use the specific wavelengths and spontaneous decay rates for the  $^{40}\text{Ca}^+$  ion, but this apart the calculations are general for alkali earth ions. All relevant parameters for the alkali earth ions can be found in ref. [31] and are reproduced in the Appendix . The detection scheme consists of two STIRAP processes. The first transfers population from  $|1\rangle$  to  $|3\rangle$  applying the  $A$  and  $B$ -fields as pump and Stokes field respectively. The

second process between  $|3\rangle$  and  $|5\rangle$  uses  $C$  as the pump field and  $D$  as the Stokes field.

We first investigate the effect of pulse delay (Sec. IV A), laser detunings (Sec. IV B), laser line width (Sec. IV C), pulse width (Sec. IV D) and residual light (Sec. IV E). All these simulations are performed on the latter transition because this transition is subject to spontaneous decay out of the system and thus has a higher sensitivity to non-adiabaticity. The simulations are made with all the population initially in  $|3\rangle$  and we find the transfer efficiency as the final population in  $|5\rangle$ . We use Gaussian pulses as defined in Eq. (4) with pulse widths  $\tau_C = \tau_D$  and we use the definitions of Sec. II with the substitution of field indexes  $A \leftrightarrow C$  and  $B \leftrightarrow D$ . An experimental investigation of this transition can be found in Ref. [29].

The first STIRAP stage is more sensitive to ion motion because the two laser fields used have very different wavelengths and the Doppler shift induced by the ion motion therefore gives a large two-photon detuning. Since this stage is responsible for the internal state selection, it is also important to investigate the effect of laser polarization errors and the resulting depletion of the wrong qubit state. The simulations of ion micro motion (Sec. IV F) and polarization errors (Sec. V) are therefore performed on the first STIRAP transition. All parameters for the simulations are mentioned in the figure captions and hence omitted in the text.

### A. Effect of pulse delay

The first parameter we investigate is the delay between the two pulses and show the transfer efficiency as a function of  $\eta$  for various peak Rabi frequencies  $\Omega_{C,0} = \Omega_{D,0}$  in Fig. 5. The simulations show that for Rabi frequencies above  $\Omega_{C,0} = \Omega_{D,0} = 2\pi \times 100$  MHz the transfer efficiency is close to unity and insensitive to fluctuations in the delay ( $P_5 > 0.999$  for fluctuations of  $\eta$  below 0.2 with respect to the optimal value of 0.85). For smaller Rabi frequencies the transfer efficiency decreases and the sensitivity to delay fluctuations increases.

The plateau of  $P_5 \simeq 0.07$  for positive  $\eta$  values is the result of optical pumping by the pump field,  $\Omega_C$ . For  $\eta > 0$  this pulse is applied last, and the Stokes field cannot repump population.

Although the results of Fig. 5 are calculated for zero one-photon detuning and hence the theory of Sec. II is not valid, we still see general trend that high Rabi frequencies are needed to maintain adiabaticity. As indicated by the crosses the delay giving maximum transfer efficiency is found to grow with increasing Rabi frequencies, consistent with Fig. 4 (a).

### B. Laser detunings

To diminish the effect of incoherent excitations we prefer large one-photon detunings of the lasers. We thus

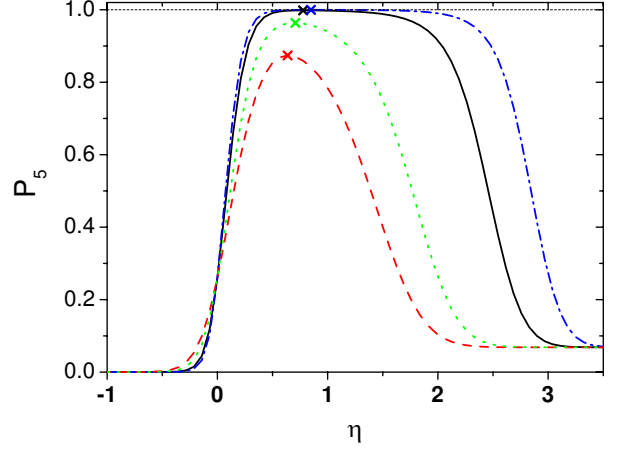


FIG. 5: (Color) Transfer efficiency as a function of delay between pulses for different choices of peak Rabi frequencies: (---)  $\Omega_{C,0} = \Omega_{D,0} = 2\pi \times 10$  MHz, (···)  $\Omega_{C,0} = \Omega_{D,0} = 2\pi \times 20$  MHz, (—)  $\Omega_{C,0} = \Omega_{D,0} = 2\pi \times 100$  MHz, (—·—)  $\Omega_{C,0} = \Omega_{D,0} = 2\pi \times 300$  MHz. Positive delay correspond to the counter intuitive pulse sequence, where the laser pulse of field  $D$  arrives before the laser pulse of field  $C$ . Parameters:  $\tau_C = \tau_D = 2 \mu\text{s}$  and  $\Delta_C = \Delta_D = 0$ .

investigate the sensitivity of STIRAP to one- and two-photon detunings. The simulations presented in Fig. 6

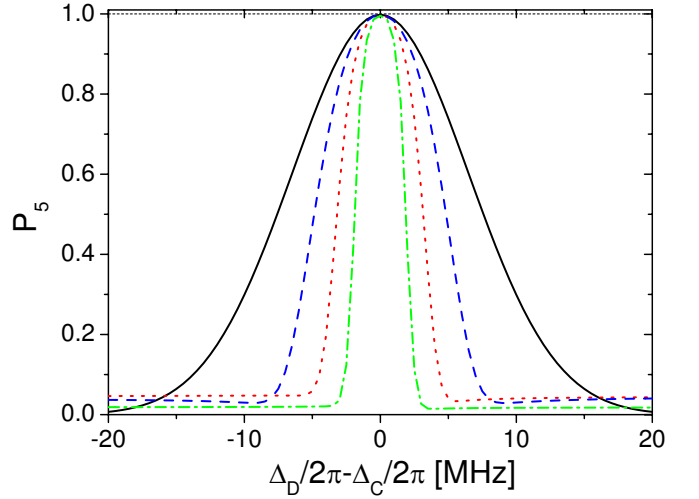


FIG. 6: (Color) Transfer efficiency as a function of two-photon detuning of the C and D lasers for different choices of one photon detuning. The simulations are made with  $\Omega_{C,0} = \Omega_{D,0} = 2\pi \times 100$  MHz,  $\tau_C = \tau_D = 2 \mu\text{s}$  and  $\Delta t = 1.2 \mu\text{s}$  ( $\eta = 0.85$ ). (—)  $\Delta_C = 0$  MHz, (—·—)  $\Delta_C = 2\pi \times 300$  MHz ( $\Lambda = 18.5$ ), (···)  $\Delta_C = 2\pi \times 600$  MHz ( $\Lambda = 9.3$ ), (···)  $\Delta_C = 2\pi \times 1200$  MHz ( $\Lambda = 4.6$ ).

show that increasing the one-photon detuning does not limit the transfer efficiency as long as we are close to the two-photon resonance. This criterion gets stricter as we increase the one-photon detuning. If we require

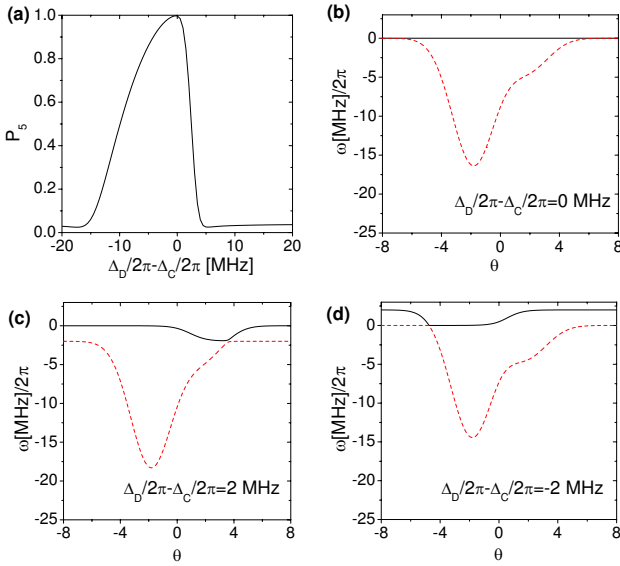


FIG. 7: (Color)(a) Transfer efficiency as a function of two-photon detuning. Evolution of eigenvalues as a function of time is shown in (b):  $\Delta_D - \Delta_C = 0$  MHz, (c)  $\Delta_D - \Delta_C = 2\pi \times 2$  MHz and (d)  $\Delta_D - \Delta_C = -2\pi \times 2$  MHz. In (b), (c) and (d) we use the signatures: (—)  $\omega^D$ , (---)  $\omega^-$ . Parameters used for all graphs:  $\Omega_{C,0} = 2\pi \times 100$  MHz,  $\Omega_{D,0} = 2\pi \times 200$  MHz,  $\Delta_C = 2\pi \times 600$  MHz,  $\tau_C = \tau_D = 2$   $\mu$ s and  $\Delta t = 1.2$   $\mu$ s ( $\Lambda = 18.5$ ,  $\eta = 0.85$ ).

$P_5 > 0.99$  the demand on two-photon detuning is  $\pm 2\pi \times 0.5$  MHz when  $\Delta_C = 2\pi \times 1200$  MHz as estimated from the dash-dotted curve of Fig. 6. For  $\Delta_C = 2\pi \times 600$  MHz, maintaining a two photon resonance within  $2\pi \times 1$  MHz is sufficient as seen from the dotted curve of Fig. 6. An efficient transfer can thus be maintained in spite of a drift from two-photon resonance making STIRAP robust with respect to small frequency drifts of the involved lasers. A closer look at Fig. 6 reveals that the spectra are not exactly symmetric with respect to the sign of the two photon detuning. With unbalanced Rabi frequencies,  $\Omega_{D,0} = 2\Omega_{C,0}$  (See. Fig. 7(a)), the asymmetry becomes more evident. For small negative two-photon detunings the transfer efficiency is much higher than for the corresponding positive two-photon detuning. This effect is due to diabatic transfer between  $|d\rangle$  and the energetically closest bright state  $|-\rangle$ . As discussed in Sec. II this is likely when  $|d\rangle$  and  $|-\rangle$  are nearly degenerate. The eigenvalues found in Eq. (2) are obtained on two photon resonance and the solutions are more complicated in the situation where this condition is not met. They have been derived in [32] and are plotted in Fig. 7. We show the eigenvalues of  $|d\rangle$  (solid curves) and  $|-\rangle$  (dashed curves) as a function of time for three different choices of two photon detuning. In the case where  $\Delta_D - \Delta_C = 0$  MHz (See Fig. 7(b)) the eigenvalues of course coincide when the Rabi frequencies are zero before and after the pulses, but in this case no diabatic transfer will occur as no coupling is present. For positive and

negative detunings ( $\Delta_D - \Delta_C = 2\pi \times 2$  MHz, Fig. 7(c) and  $\Delta_D - \Delta_C = -2\pi \times 2$  MHz, Fig. 7(d)) we see avoided crossings leading to a probability for diabatic transfer to the  $|-\rangle$ -state. This leads to population of the  $|4\rangle$ -state, which decays rapidly and the population mainly ends up in  $|1\rangle$ . When the energy splitting between the  $|d\rangle$  and the  $|-\rangle$  state is small maintaining adiabaticity requires high coupling strengths. For a positive two-photon detuning the avoided crossing occurs late in the sequence, as shown in Fig. 7(c). Here the coupling strength is relatively small due to  $\Omega_{D,0} = 2\Omega_{C,0}$ , hence the probability of diabatic transfer is large. With a negative two-photon detuning the avoided crossing occurs early, as shown in Fig. 7(c). The coupling is stronger at this time and the probability of diabatic transfer is thus smaller. This difference gives rise to the asymmetry of the spectra in Fig. 7(a).

### C. Laser line widths

Laser phase fluctuations lead to dephasing between the three states involved and therefore may affect STIRAP. The dephasing effect has been studied thoroughly in [33], where the STIRAP transfer efficiency has been shown to depend only on the dephasing rate between  $|3\rangle$  and  $|5\rangle$ ,  $\gamma_{35}$ .

$$P_5 = \frac{1}{3} + \frac{2}{3} e^{-3\gamma_{35}\tau^2/16\Delta t}, \quad (19)$$

for Gaussian pulses within the adiabatic limit, not taking decay from  $|4\rangle$  into account. In Fig. 8 we present simulations showing the exact influence of the laser phase fluctuations together with Eq. (19). This shows that

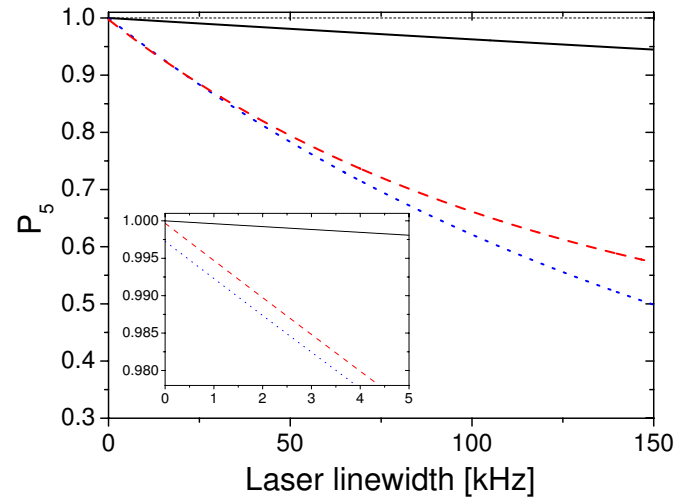


FIG. 8: (Color) Transfer efficiency as a function of the line width of the C and D laser fields for different choices of Rabi frequencies. The simulations use  $\tau_C = \tau_D = 2$   $\mu$ s,  $\Delta t = 1.2$   $\mu$ s ( $\eta = 0.85$ ) and  $\Delta_C = \Delta_D = 2\pi \times 600$  MHz. (—)  $P_5 = 1/3 + 2/3 \exp(-3\gamma_{35}\tau^2/16\Delta t)$ , (---)  $\Omega_{C,0} = \Omega_{D,0} = 2\pi \times 300$  MHz ( $\Lambda = 83.3$ ), (••)  $\Omega_{C,0} = \Omega_{D,0} = 2\pi \times 100$  MHz ( $\Lambda = 9.3$ ).

the transfer efficiency is strongly limited by the laser phase fluctuations and because of the non-zero decay from  $|4\rangle$  the situation is even worse than predicted in Eq. (19). For high Rabi frequencies the coupling is stronger and therefore the limitations due to dephasing are less pronounced. To maintain a transfer efficiency above 0.99 we require laser line widths below  $2\pi \times 1.5$  kHz for  $\Omega_{C,0} = \Omega_{D,0} = 2\pi \times 100$  MHz and below  $2\pi \times 2$  kHz for  $\Omega_{C,0} = \Omega_{D,0} = 2\pi \times 300$  MHz. It should be noted that we by laser line width here mean the line width integrated over the course of the experiment. This is not necessarily the steady state laser line width. For pulse sequences of roughly 10  $\mu$ s duration, as are employed in our simulations, laser line widths of a few kHz are not unrealistic.

#### D. Role of pulse widths

As discussed above the laser phase fluctuations limit the transfer efficiency making it preferable to use short pulses. Short pulses however require high Rabi frequencies to maintain the adiabaticity. In Fig. 9 we show the transfer efficiency as a function of pulse width in the case of no laser line width as well as the case of a  $2\pi \times 2$  kHz line width. As expected, for the case of no line width we find an increasing efficiency as we increase the pulse widths because the criterion for adiabaticity is better fulfilled for larger pulse widths as found in (11). We indicate the point where we exceed 0.995 on the graph. When we introduce a  $2\pi \times 2$  kHz laser line width we find an optimum as indicated on the graph.

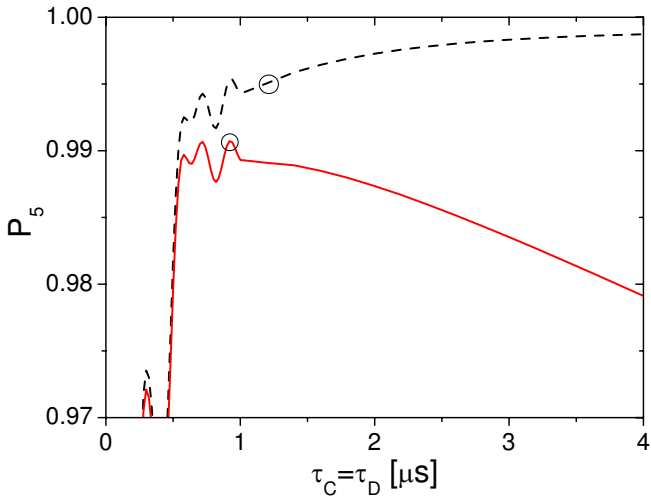


FIG. 9: (Color) Transfer efficiency as a function of pulse width of the  $C$  and  $D$  laser fields for  $2\pi \times 2$  kHz (—) as well as no laser line width (---). The delay between the pulses is given by  $\eta = 0.85$ , laser detunings are  $\Delta_C = \Delta_D = 2\pi \times 600$  MHz and peak Rabi frequencies  $\Omega_{C,0} = \Omega_{D,0} = 2\pi \times 100$  MHz ( $\Lambda = 9.3$ ).

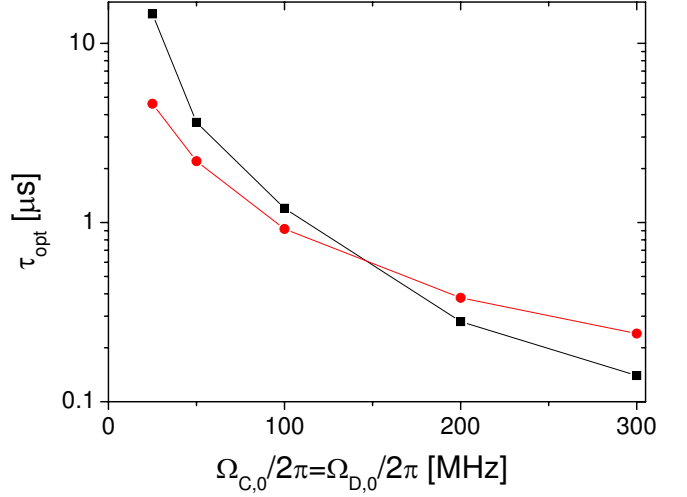


FIG. 10: (Color) Optimal pulse width as a function of Rabi frequency of the  $C$  and  $D$  laser fields for  $2\pi \times 2$  kHz (●) as well as no laser line width (■). The delay between the pulses is given by  $\eta = 0.85$ , laser detunings are  $\Delta_C = \Delta_D = 2\pi \times 600$  MHz.

This optimum depends on the Rabi frequencies of the lasers and we find it for different Rabi frequencies as pictured in Fig. 10. In the case of no line width we plot the pulse widths required to exceed a 0.995 transfer efficiency. The optimal choice of pulse width is then shown to depend of the Rabi frequency and the line width of the STIRAP laser fields. Also with respect to pulse width STIRAP is found to be a robust method.

In the calculations leading to Fig. 10 we have assumed the laser line widths to be constant over the range of pulse durations involved. More realistically one would expect the laser line widths to grow proportional to  $(\tau_{C,D})^\alpha$ , where the power,  $\alpha$ , is in the range  $0.5 \rightarrow 1$  for a phase diffusion process.

#### E. Residual light

In the first generation of STIRAP experiments beams of atoms passed through two stationary laser beams [20, 22] and in this case no residual light was present, but when we consider the situation with stationary ions and pulsed laser beams the situation is less favorable. In case of a constant background level of laser light, the ions do not start out in an exact dark state and hence population transfer may be limited by the resulting finite population of the short lived states  $|2\rangle$  and  $|4\rangle$ . Moreover, since the residual light is able to excite the Raman resonance between the  $|3\rangle$  and the  $|5\rangle$  states, repumping of the transferred population can take place after ended STIRAP pulse sequence. With a small background level of light this Raman resonance will be narrow and hence the limitation of population transfer is most severe near two-photon resonance as experimentally found

in [29]. We denote the Rabi frequency of the residual light  $\Omega_{\text{off},i}$ ,  $i = \{A, B, C, D\}$ . We first look at the transfer efficiency as a function of the two-photon detuning. When no residual light is present the transfer efficiency is optimal on two-photon resonance as shown previously in Fig. 6, but this is no longer the case, when we introduce a fraction of residual light,  $\Omega_{\text{off},i}/\Omega_{i,0}$ . In Fig. 11(a) we present the transfer efficiency as function of two-photon detuning for different fractions of residual light. As we increase this fraction we see an increasing loss of population on two-photon resonance. With  $\Omega_{\text{off},i}/\Omega_{i,0}$  less than 0.02 (dashed curves) this loss is only a few percent relative to the maximum transfer efficiency. However already with  $\Omega_{\text{off},i}/\Omega_{i,0} = 0.05$  (solid curve) the loss has grown to nearly 50 % near two-photon resonance, rendering the detection scheme useless in this case.

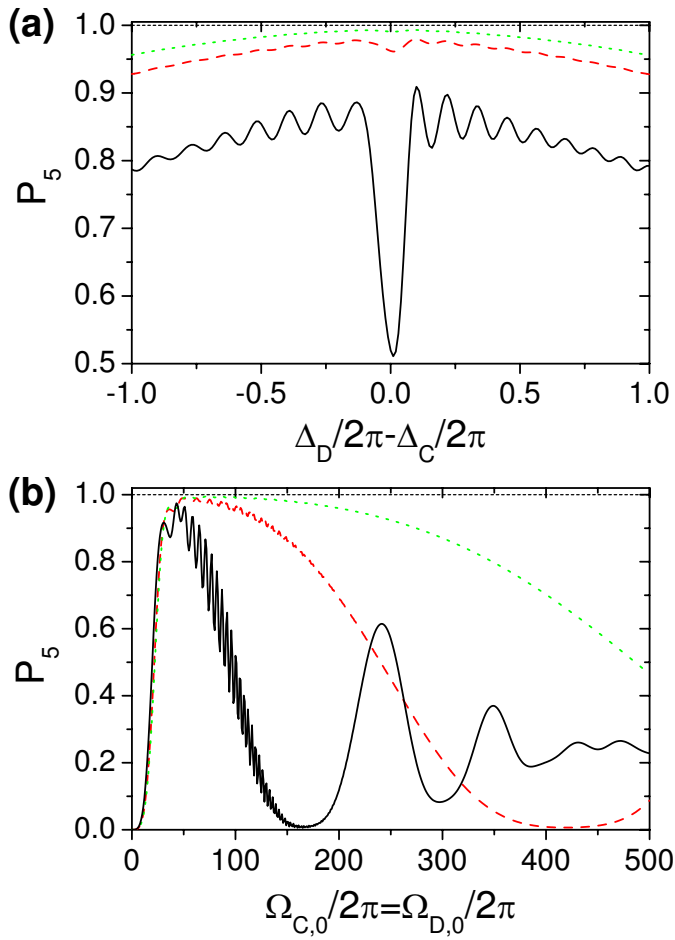


FIG. 11: (Color) (a) Transfer efficiency as a function of two-photon detuning with  $\Omega_{C,0} = \Omega_{D,0} = 2\pi \times 100$  MHz and  $\Delta_C = 2\pi \times 600$  MHz.  $\Lambda = 9.3$ . (b) Transfer efficiency as the peak Rabi frequencies are varied simulated with  $\Delta_C = \Delta_D = 2\pi \times 600$  MHz. The different curves represent different fractions of residual light: (---)  $\Omega_{\text{off},i}/\Omega_{i,0} = 0.01$ , (- - -)  $\Omega_{\text{off},i}/\Omega_{i,0} = 0.02$  and (—)  $\Omega_{\text{off},i}/\Omega_{i,0} = 0.05$ . Parameters used in simulations:  $\tau_C = \tau_D = 2$   $\mu$ s,  $\Delta t = 1.2$   $\mu$ s, yielding  $\eta = 0.85$ . The total time duration is 20  $\mu$ s and laser line width has been ignored.

Residual light is typically present as a fraction of the peak Rabi frequencies, and hence very high Rabi frequencies are not necessarily preferable. In Fig. 11(b) we show the transfer efficiency as a function of the peak Rabi frequencies in the STIRAP pulses for different choices of the fraction of residual light. Increasing the Rabi frequencies increases the transfer efficiency until the residual light limits the transfer. For even higher Rabi frequencies we observe Rabi-flopplings between  $|3\rangle$  and  $|5\rangle$ .

## F. Ion motion

The ions have so far been considered as having no motion with respect to the laser fields. We consider the ions to be confined in a linear Paul trap [34], where they experience an effective confining potential due to RF- and DC-fields. The ion motion can be derived to consist of a three dimensional harmonic motion at frequencies  $\omega_x$ ,  $\omega_y$  and  $\omega_z$  called the secular motion [34]. In addition the RF-field drives an oscillation at the RF-frequency,  $\Omega_{RF}$ . This oscillation is called the ion micro motion. The secular frequencies are typical much smaller than  $\Omega_{RF}$  making the micro motion the most critical with respect to the STIRAP transfer efficiency. The effect of micro motion is simulated by modulating the detunings as

$$\Delta_i(t) = \Delta_i(0) - v \frac{2\pi}{\lambda_i} \cos(\Omega_{RF}t). \quad (20)$$

We consider only micro motion in one dimension with maximum velocity  $v$ . This classical treatment of micro motion is justified by quantum Monte Carlo simulations where the ion motion has been quantized showing no effect on the transfer efficiency [35]. Another argument for this classical simplification is the strength of the laser fields making  $\Omega_{i,0} \gg \Omega_{RF}$ . As discussed previously, the STIRAP transfer efficiency is more sensitive to two-photon than one-photon detunings. If we assume co-propagating laser fields and take the  $^{40}\text{Ca}^+$  ion as an example, the two photon detuning will be strongly modulated in the case of the  $|1\rangle$ - $|2\rangle$ - $|3\rangle$  transition where the two laser fields have a large wavelength difference ( $\Delta\lambda/\lambda$ )<sub>123</sub> = 0.54, while the  $|3\rangle$ - $|4\rangle$ - $|5\rangle$  transition experiences a much smaller modulation of the two-photon detuning ( $\Delta\lambda/\lambda$ )<sub>345</sub> = 0.005. This means that the first transition is strongly limited by micro motion while the second remains virtually unaffected.

In Fig. 12 we show the transfer efficiency as a function of the micro motion velocity for different choices of detuning. The simulations show that when we increase the one-photon detuning the micro motion velocity becomes an increasingly limiting factor. For small micro motion velocities we see that the transfer efficiency is higher for small one-photon detunings. This is due to an decreased sensitivity to a non-vanishing two-photon detuning as discussed in Sec. IV B. For higher velocities the one-photon detuning is strongly modulated. This results in sidebands of which the high frequency component comes

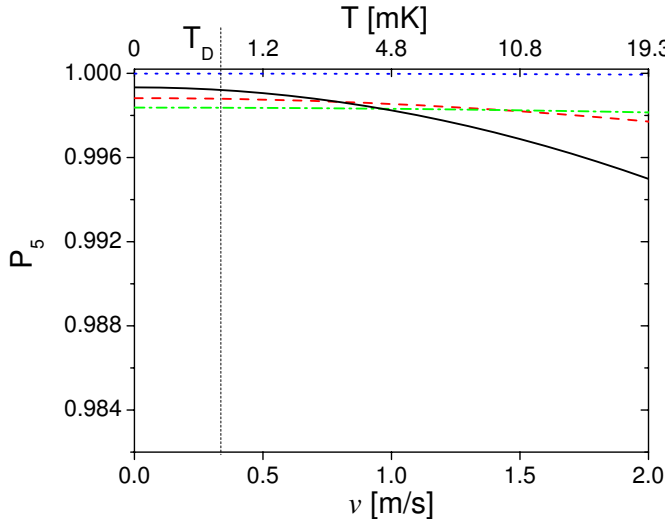


FIG. 12: (Color) Transfer efficiency as a function of the micro motion velocity. The different curves show results for different detunings: (•)  $\Delta_A = \Delta_B = 0$  MHz, (—)  $\Delta_A = \Delta_B = 2\pi \times 300$  MHz ( $\Lambda = 18.5$ ), (---)  $\Delta_A = \Delta_B = 2\pi \times 600$  MHz ( $\Lambda = 9.3$ ) and (---)  $\Delta_A = \Delta_B = 2\pi \times 1200$  MHz ( $\Lambda = 4.6$ ). Parameters used for simulations:  $\tau_A = \tau_B = 2$   $\mu$ s,  $\Delta t = 1.3$   $\mu$ s ( $\eta = 0.92$ ),  $\Omega_A = \Omega_B = 2\pi \times 100$  MHz and  $\Omega_{RF} = 2\pi \times 16.8$  MHz. The temperature of the ion is defined as  $T = mv^2/k_B$ , where  $m$  is the ion mass and  $k_B$  Boltzmann's constant. The Doppler temperature for  $\text{Ca}^+$ ,  $T_D$ , is indicated by the vertical line.

close to resonance, hereby inducing real transitions to the short lived  $|2\rangle$ -state. This effect gets more evident when the one-photon detuning is close to  $v\frac{2\pi}{\lambda_i}$ , which for our parameters varies between 0 and 100 MHz. Fig. 12 shows small sensitivity to micro motion for very small and very large values of  $\Delta_A = \Delta_B$ , while the  $\Delta_A = \Delta_B = 300$  MHz trace shows a rapid drop as a function of  $v$ . For the chosen parameters a micro motion velocity below 1 m/s ensures a transfer efficiency above 0.998. From the kinetic energy of the ion a temperature can be defined through the relation  $\frac{1}{2}k_B T = \frac{1}{2}mv^2$ . Hence, in the case of  $^{40}\text{Ca}^+$  a velocity below 1 m/s correspond to a temperature below 4.8 mK. When the ion is Doppler laser cooled temperatures below the so called Doppler temperature,  $T_D$  can not be obtained. For  $^{40}\text{Ca}^+$   $T_D = 0.5$  mK as indicated by the vertical line on Fig. 12. This is well below the required 4.8 mK and Doppler cooling is thus sufficient to achieve a high transfer efficiency. Doppler temperatures for other relevant ions can be found in Table I.

## V. POLARIZATION REQUIREMENTS

Until this point other Zeeman sublevels have been ignored, however in order to investigate the effect of laser polarization deviating from purely circular we now introduce all of these in the first stage STIRAP. The optical

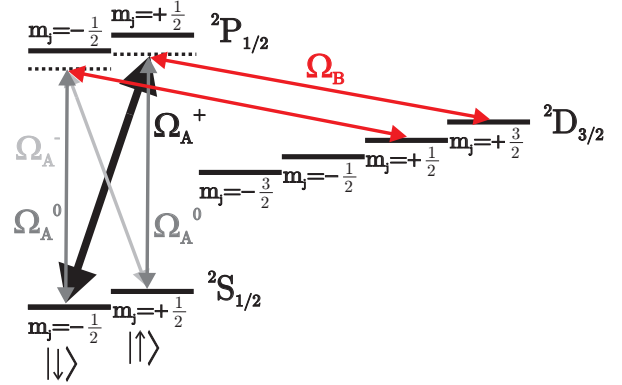


FIG. 13: (Color) Zeeman sublevels of the three states involved in the first STIRAP process. The  $S_{1/2}$  and  $P_{1/2}$  states are coupled by a laser field with a  $\sigma_+$  polarized component ( $\Omega_A^+$ ), a  $\sigma_-$  polarized component ( $\Omega_A^-$ ) and a  $\pi$  polarized component ( $\Omega_A^0$ ). The  $D_{3/2}$  and  $P_{1/2}$  states are coupled by a laser field ( $\Omega_B$ ) with a pure  $\sigma_-$  polarization.

Bloch equations for the full 8 level system are derived analogous to the equations in Sec. III. We consider the field  $A$  to have both  $\sigma_{\pm}$  polarization components as well as a  $\pi$  component in case of magnetic field errors. The second STIRAP field,  $B$ , is assumed to have perfect  $\sigma_-$  polarization. We denote the  $\sigma_+$  polarized component of  $\Omega_A$ ,  $\Omega_A^+$ , the  $\sigma_-$  polarized component  $\Omega_A^-$  and the  $\pi$  polarized component  $\Omega_A^0$  (See Fig. 13).

Efficient qubit projection requires all population moved from  $|\downarrow\rangle$  to the  $D_{3/2}$  levels while leaving the  $|\uparrow\rangle$  population unchanged. In order to test these criteria we simulate the problem with two different initial states corresponding to all population in  $|\downarrow\rangle$  and  $|\uparrow\rangle$  respectively. The results are shown in Fig. 14. First we focus on the situation, where all initial population is in the  $|\downarrow\rangle$  qubit state. Ideally the final populations in both qubit states should be vanishing for our scheme to work. The results, shown in Fig. 14 (a) and (b), reveal that detection errors can be kept below 0.01 provided the magnetic field can be controlled accurately enough to keep  $\Omega_A^0/\Omega_A^+$  below 0.02. However, when all initial population is in the  $|\uparrow\rangle$  state, the situation is worse. From Fig. 14 (c), we find that the population in the  $|\uparrow\rangle$  state is pumped out as the relative amplitude of the  $\sigma_-$  polarized component is increasing. This is of course undesired. Hence, in order to keep qubit detection errors below 0.01 for an arbitrary initial state, we must demand that  $\Omega_A^0/\Omega_A^+ < 0.02$  and  $\Omega_A^-/\Omega_A^+ < 0.04$  with the parameters used in this simulation.

## VI. FULL SIMULATION

Finally, we present the results of a simulation of the full two stage STIRAP population transfer including all of the above described effects except polarization errors. The parameters relevant to the simulation can be found

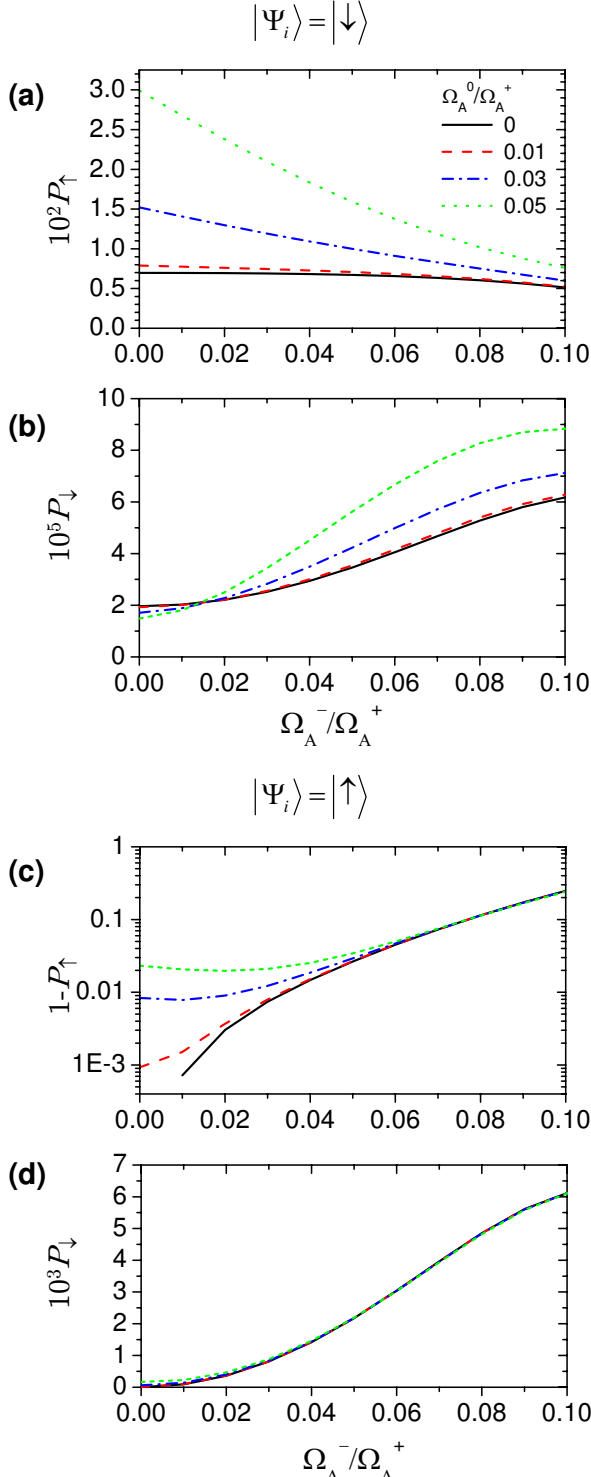


FIG. 14: (Color) Effect of polarization error and error in magnetic field direction. Populations of the qubit states  $|\downarrow\rangle$ ,  $P_\downarrow$ , and  $|\uparrow\rangle$ ,  $P_\uparrow$ , plotted as function of the relative  $\sigma_-$  polarization component,  $\Omega_A^-/\Omega_A^+$ . The various curves on each plot correspond to different magnetic field direction errors, parameterized by the relative  $\pi$  polarization component,  $\Omega_A^0/\Omega_A^+$ . (—)  $\Omega_A^0/\Omega_A^+ = 0$ , (---)  $\Omega_A^0/\Omega_A^+ = 0.01$ , (----)  $\Omega_A^0/\Omega_A^+ = 0.03$  and (----)  $\Omega_A^0/\Omega_A^+ = 0.05$ . The upper two graphs, (a) and (b), correspond to all initial population in the  $|\downarrow\rangle$  qubit state, while the lower two graphs, (c) and (d), correspond to all initial population in  $|\uparrow\rangle$ . The parameters for the simulations are  $\Omega_{A,0}^+ = \Omega_{B,0} = 2\pi \times 300$  MHz,  $\Delta_A = \Delta_B = 2\pi \times 300$  MHz,  $\tau = 2$   $\mu$ s and  $\Delta t = 1.3$   $\mu$ s. ( $\Lambda = 167$ ,  $\eta = 0.92$ ).

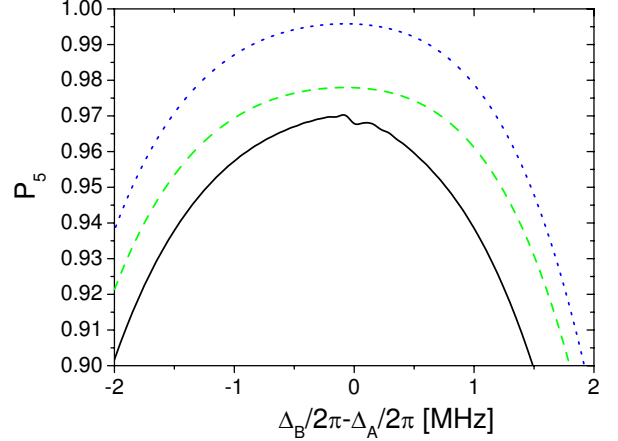


FIG. 15: (Color) Full simulation of the two stage STIRAP. The plot shows the population transfer as function of two photon detuning of the first STIRAP stage. Parameters are:  $\Delta_A = \Delta_C = \Delta_D = 2\pi \times 600$  MHz,  $\Omega_A = \Omega_B = \Omega_C = \Omega_D = 2\pi \times 100$  MHz,  $\tau_A = \tau_B = \tau_C = \tau_D = 2\mu$ s. All laser line widths are  $2\pi \times 2$  kHz and the trap is characterized by  $\Omega_{RF} = 2\pi \times 16.7$  MHz and  $v = 0.4$  m/s, corresponding to a temperature of 0.8 mK. The STIRAP's have  $\Delta t = 1.2\mu$ s corresponding to  $\eta = 0.85$  and  $\Lambda = 9.3$  for both stages. The two STIRAP stages are separated by 10  $\mu$ s and the overall simulation time is 30  $\mu$ s. The Rabi frequencies associated with the residual power are 0.01 relative to the peak Rabi frequencies for all four fields. The curves correspond to: (—) all effects on, (---) residual power set to zero but laser line width on, and (----) both laser line width and residual power set to zero.

in the caption of Fig. 15. The figure shows the population transfer efficiency as function of the two photon detuning,  $\Delta_B - \Delta_A$ , for the first STIRAP stage. Assuming that the ions can be kept cooled close to the Doppler temperature, we have chosen a temperature due to the micro motion of 0.8 mK for this simulation. The resulting peak velocity of 0.4 m/s results in a loss of population transfer of less than 0.01 according to the discussion of Sec. IV F. The two photon detuning of the second STIRAP stage has been chosen to be zero and the residual power level is chosen to yield a Rabi frequency of 0.01 relative to the peak Rabi frequencies for all four optical fields.

From Fig. 15 we find, when all effects are taken into account, a maximum transfer efficiency of 0.97 for  $\Delta_B - \Delta_A = -2\pi \times 0.09$  MHz. This corresponds to the full, black curve. In order to identify the processes limiting this efficiency we show on the green, dashed curve the resulting efficiency when the residual optical power is set to zero. Comparison with the full curve shows that a loss in efficiency of almost 0.01 can be attributed to repumping by residual laser light. The blue, dotted curve of Fig. 15 shows the transfer efficiency when both residual light and laser line widths are set to zero. Here a maximum transfer efficiency of 0.996 is found near two photon resonance indicating that the finite laser line width is indeed

a deleterious effect to STIRAP. The line width of 2 kHz assigned to all lasers in the simulation results in a loss of transfer efficiency of nearly 0.02. In order to reduce the effect of laser phase fluctuations shorter pulse durations and consequently higher Rabi frequencies must be used.

The simulation illustrates the importance of efficient switching on and off laser power in the STIRAP process. Unless the lasers involved in the two STIRAP stages are pairwise phase locked one obviously needs fairly high intensities of the optical pulses and hence the requirements to the residual laser power become more stringent. However, as can be seen from Fig. 5, it is noted that the scheme is insensitive to *fluctuations* in the laser power as long as the transitions involved are well saturated and adiabaticity is maintained.

## VII. SUMMARY AND CONCLUSIONS

In summary, we analyze the scheme where two magnetic sublevels of the  $S_{1/2}$  ground state of alkali earth ions are considered as qubit states. We have shown that qubit projection can be effectively performed by electronically shelving the population of one magnetic sublevel via a double STIRAP process. Hereby the population is transferred to the metastable  $D_{5/2}$  state and remaining population of the other qubit state can hence be detected by driving the strong Doppler cooling transition of the ions and spatially monitoring the fluorescence. In order to selectively shelve only one qubit state we apply appropriately polarized light in the first STIRAP process.

We have established the formalism describing the system consisting of the 5 energetically lowest levels of the alkali earth ions and we model the STIRAP processes using Gaussian shaped pulses from partially phase coherent lasers. Specific simulations have been performed by solving the optical Bloch equations for the  $^{40}\text{Ca}^+$  ion from which we conclude that our scheme is indeed feasible with a projection efficiency exceeding 99 %, provided laser linewidths can be kept below 1.5 kHz over the timescale of the pulse sequence. In practice a high efficiency requires Rabi frequencies in the 100's of MHz regime in order to maintain adiabaticity of the ions during the short timespan, the shelving is allowed to take, before the lasers decohere. However, since we are driving strong, dipole allowed transitions, such high Rabi frequencies can be achieved by using moderately focused lasers with 5-10 mWatts of power.

In order to avoid unwanted excitations, we assume all lasers to be detuned roughly 0.5 - 1 GHz from the one photon resonance. In the limit of this detuning dominating over Rabi frequencies, we have identified the adiabaticity criteria for the ions when Gaussian light pulses are applied. Given an available laser power and hence certain Rabi frequencies, we find an optimum pulse separation depending only on the parameter  $\Lambda$ , proportional to the number of Raman Rabi cycles during the STIRAP,

and the ratio of the Rabi frequencies involved the process. Within variations of 20 % we find the optimum pulse separation to be  $\tau/\sqrt{2}$ , where  $\tau$  is the  $1/e$  full width of the Gaussian pulses.

In contrast to early STIRAP experiments, where atomic beams and stationary laser beams were used, our system involves stationary atoms and laser pulses. Hence, efficient switching on and off of light is required. In practice this is a nontrivial task to perform on a microsecond timescale, thus, we have analyzed the effect of residual light irradiating the ions during and after the electronic shelving. This is found to pose a serious problem to the shelving efficiency, and it is likely to be the main limiting factor to the quality of qubit projection.

Motion in the ion trap is included in the analysis, and found to be unimportant close to the Doppler cooling limit. For calcium ions this is 0.5 mK.

Finally, we have analysed the effect of impure polarization of light. This could come about from stray birefringence or variations in the direction of an external magnetic field. Solutions to the optical Bloch equations involving magnetic sublevels of the 3 lowest states of the calcium ion show, that projection errors can be kept below 0.01 provided the relative Rabi frequencies of the unwanted polarization components can be kept below 0.02-0.04.

A simulation including all effects outlined above except polarization errors showed the importance of being able to efficiently switching on and off laser power as well as using highly coherent or preferably phase locked lasers in this qubit detection scheme. Since we assume the lasers involved in the scheme are only partially coherent a loss of transfer efficiency of almost 0.02 was found for laser line widths of 2 kHz over the time of the experiment. Performing the shelving on a shorter timescale will obviously reduce the relevant line widths but also require higher Rabi frequencies and consequently better suppression of residual laser light.

## APPENDIX: RELEVANT ION DATA

Table I shows spectroscopic data for some selected ions possessing the level structure and transitions shown in Fig. 1. Listed are wavelengths,  $\lambda_i$  associated with the fields  $\Omega_i$ ,  $i = \{A, B, C, D\}$ , decay rates of the short lived states  $|2\rangle$  and  $|4\rangle$  into the stable and metastable states and the Doppler temperature,  $T_D$ . The data is reproduced from Ref. [31].

## ACKNOWLEDGMENTS

This work has been supported by the Danish National Research Council and by the Carlsberg Foundation.

TABLE I: Data of some relevant ions

Property	$^{40}\text{Ca}^+$	$^{88}\text{Sr}^+$	$^{138}\text{Ba}^+$	$^{198,200,202}\text{Hg}^+$
$\lambda_A$ [nm]	397	422	493	194
$\lambda_B$ [nm]	866	1092	650	10670
$\lambda_C$ [nm]	850	1004	585	991
$\lambda_D$ [nm]	854	1033	614	398
$\Gamma_{21}/2\pi$ [MHz]	21	20	14	69
$\Gamma_{23}/2\pi$ [MHz]	1.7	1.5	5.3	0.05
$\Gamma_{43}/2\pi$ [MHz]	0.18	0.18	0.76	0.48
$\Gamma_{45}/2\pi$ [MHz]	1.6	1.4	5.9	40
$T_D$ [mK]	0.50	0.49	0.35	1.7

[1] M. A. Nielsen and I. L. Chuang, *Quantum Computation and Quantum Information* (Cambridge University Press, Cambridge, 2000).

[2] A. Wallraff, D. I. Schuster, A. Blais, L. Frunzio, J. Majer, M. H. Devoret, S. M. Girvin, and R. J. Schoelkopf, *Phys. Rev. Lett.* **95**, 060501 (2005).

[3] M. Steffen, M. Ansmann, R. C. Bialczak, N. Katz, E. Lucero, R. McDermott, M. Neeley, E. M. Weig, A. N. Cleland, and J. M. Martinis, *Science* **313**, 1423 (2006).

[4] M. Atature, J. Dreiser, A. Badolati, A. Hogen, K. Karrai, and A. Imamoglu, *Science* **312**, 551 (2006).

[5] E. Knill, R. LaFlamme, and G. J. Milburn, *Nature* **409**, 46 (2001).

[6] R. Prevedel, P. Walther, F. Tiefenbacher, P. Bohi, R. Kaltenbaek, T. Jennewein, and A. Zeilinger, *Nature* **445**, 65 (2007).

[7] Q. A. Turchette, C. J. Hood, W. Lange, H. Mabuchi, and H. J. Kimble, *Phys. Rev. Lett.* **75**, 4710 (1995).

[8] D. Schrader, I. Dotsenko, M. Khudaverdyan, Y. Miroshnychenko, A. Rauschenbeutel, and D. Meschede, *Phys. Rev. Lett.* **93**, 150501 (2004).

[9] J. Mompart, K. Eckert, W. Ertmer, G. Birk, and M. Lewenstein, *Phys. Rev. Lett.* **90**, 147901 (2003).

[10] I. H. Deutsch, G. K. Brennen, and P. S. Jessen, *Fortschr. Phys.* **48**, 9 (2000).

[11] D. J. Wineland, M. Barrett, J. Britton, J. Chiaverini, B. DeMarco, W. M. Itano, B. Jelenkovic, C. Langer, D. Leibfried, V. Meyer, et al., *Phil. Trans. R. Soc. Lond. A* **361**, 1349 (2003).

[12] C. Monroe, D. M. Meekhof, B. E. King, W. M. Itano, and D. J. Wineland, *Phys. Rev. Lett.* **75**, 4714 (1995).

[13] F. Schmidt-Kaler, H. Häffner, M. Riebe, S. Gulde, G. P. T. Lancaster, T. Deuschle, C. Becher, C. F. Roos, J. Eschner, and R. Blatt, *Nature* **422**, 408 (2003).

[14] D. Leibfried, E. Knill, S. Seidelin, J. Britton, R. B. Blakestad, J. Chiaverini, D. B. Hume, W. M. Itano, J. D. Jost, C. Langer, et al., *Nature* **438**, 639 (2005).

[15] H. Haffner, W. Hansel, C. F. Roos, J. Benhelm, D. Chekalakar, M. Chwalla, T. Korber, U. D. Rapol, M. Riebe, P. O. Schmidt, et al., *Nature* **438**, 643 (2005).

[16] J. Chiaverini, D. Leibfried, T. Schaetz, M. D. Barrett, R. B. Blakestad, J. Britton, W. M. Itano, J. D. Jost,

E. Knill, C. Langer, et al., *Nature* **432**, 602 (2004).

[17] D. Møller, L. B. Madsen, and K. Mølmer, *Phys. Rev. A* **75**, 062302 (2007).

[18] P. Staunum and M. Drewsen, *Phys. Rev. A* **66**, 040302(R) (2002).

[19] J. Oreg, F. T. Hioe, and J. H. Eberly, *Phys. Rev. A* **29**, 690 (1984).

[20] K. Bergmann, H. Theuer, and B. W. Shore, *Rev. Mod. Phys.* **70**, 1003 (1998).

[21] P. Staunum, Ph.D. thesis, University of Aarhus (2004).

[22] U. Gaubatz, P. Rudecki, S. Schiemann, and K. Bergmann, *J. Chem. Phys.* **92**, 5363 (1990).

[23] L. S. Goldner, C. Gerz, R. J. C. Spreeuw, S. L. Rolston, C. I. Westbrook, W. D. Phillips, P. Marte, and P. Zoller, *Phys. Rev. Lett.* **72**, 997 (1994).

[24] J. Lawall and M. Prentiss, *Phys. Rev. Lett.* **72**, 993 (1994).

[25] M. Weitz, B. C. Young, and S. Chu, *Phys. Rev. A* **50**, 2438 (1994).

[26] T. Cubel, B. K. Teo, V. S. Malinovsky, J. R. Guest, A. Reinhard, B. Knuffman, P. R. Berman, and G. Raithel, *Phys. Rev. A* **72**, 023405 (2005).

[27] B. Broers, H. B. van Linden van den Heuvell, and L. D. Noordam, *Phys. Rev. Lett.* **69**, 2062 (1992).

[28] J. Deiglmayr, M. Reetz-Lamour, T. Amthor, S. Westermann, A. L. de Oliveira, and M. Welschmuller, *Opt. Commun.* **264**, 293 (2006).

[29] J. L. Sørensen, D. Møller, T. Iversen, J. B. Thomsen, F. Jensen, P. Staunum, D. Voigt, and M. Drewsen, *New J. Phys.* **8**, 261 (2006).

[30] B. W. Shore, K. Bergmann, A. Kuhn, S. Schiemann, J. Oreg, and J. H. Eberly, *Phys. Rev. A* **45**, 5297 (1992).

[31] D. F. V. James, *Appl. Phys. B* **66**, 181 (1998).

[32] M. P. Fewell, B. W. Shore, and K. Bergmann, *Aust. J. Phys.* **50**, 281 (1997).

[33] P. A. Ivanov, N. V. Vitanov, and K. Bergmann, *Phys. Rev. A* **70**, 063409 (2004).

[34] P. Ghosh, *Ion Traps* (Clarendon Press, Oxford, 1995).

[35] J. Thomsen, *Master thesis*, Department of Physics and Astronomy (University of Aarhus, 2005).